

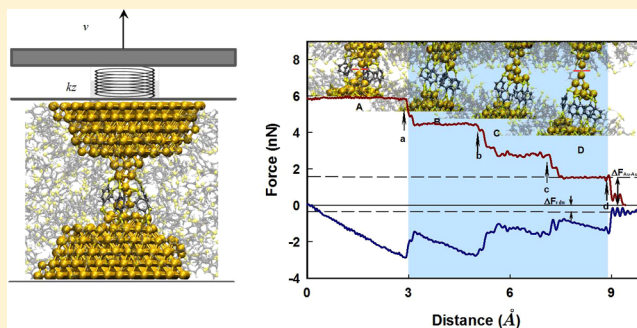
# Gold/Benzenedithiolate/Gold Molecular Junction: A Driven Dynamics Simulation on Structural Evolution and Breaking Force under Pulling

Huachuan Wang and Yongsheng Leng\*

Department of Mechanical and Aerospace Engineering, The George Washington University, 801 22nd Street NW, Washington, District of Columbia 20052, United States

## Supporting Information

**ABSTRACT:** Dynamic evolutions of molecular binding structures and breaking forces of gold/thiolate molecular junctions under pulling are still not well understood. We perform driven dynamics simulations to show that there are essentially two distinct breaking force traces corresponding to the Au–Au and Au–S bond ruptures. The latter is attributed to the formation and breaking of an additional “–Au–SR–Au–” unit in the molecular junction. The force histogram shows two force quanta at 1.5 and 2.0 nN, corresponding to the Au–Au and Au–S bond breaking. Our findings provide new molecular insights into the gold–thiolate interactions. The intermediate metal–molecule–metal binding structures could be used for further molecular transport calculations.



## 1. INTRODUCTION

Understanding the dynamic evolutions of molecular binding structures and breaking forces of single metal–molecule–metal junctions under pulling is one of the key elements in the fundamental study of molecular electronics devices.<sup>1,2</sup> The simultaneous measurements of the breaking force and electrical conductance<sup>3–6</sup> of a molecular junction enable one to characterize both mechanical and electrical properties of these novel junctions and to understand the correlation between the two properties. Compared with solely experimental measurements of molecular conductance,<sup>7–11</sup> measurements of the force/conductance variations versus the pulling distance by an atomic force microscope (AFM)<sup>3,5</sup> provide new insights into the single molecular properties at metal–organic interfaces; however, one piece of critical information, the atom-resolved binding structure of a metal–molecule–metal junction and its structural evolution under pulling, is still not attainable by this experimental technique. This is also true for the conductance measurement by the widely used mechanically controllable break junction (MCBJ) technique.<sup>7,11</sup>

The lack of this critical information directly impacts the electron-transport calculations of molecular junctions. While in many computational studies<sup>12–16</sup> the metal–molecule–metal junction was simplified as either a single molecule sandwiched between two flat metal surfaces or between two apexes of metal leads, there were always discrepancies between the electronic-transport calculations and experimental measurements of conductance. To some extent, these disagreements were attributed to the unknown binding structures of metal–molecule–metal junctions, which were largely assumed a priori in molecular transport calculations. Although this problem has

recently been explored by the DFT-based molecular dynamics (MD) simulations for relatively small systems<sup>17,18</sup> and by the classical-level MD simulations for more complicated large systems,<sup>19,20</sup> the fundamental question concerning the structure–force correlation has not yet been fully explored.

Interpretation of conductance transition was also based on perceptions of structural changes of molecular binding configurations. For example, in previous experimental studies on the molecular conductance of gold–dithiolate–gold molecular junctions, a prominent explanation to the high-to-low conductance transition was attributed to the S migrations from the “on-hollow” to the “on-top” site of S–Au binding.<sup>4</sup> This interpretation, however, was not supported by recent DFT calculations.<sup>13,20</sup> Conductance transition was also attributed to the disappearance of van der Waals interactions at metal–organic interfaces<sup>5</sup> or to the binding geometry changes from the direct thiolate–gold contact to the formation of a polymeric SR–Au(I)–SR unit, in which the formally oxidized Au(I) atom was chemically bonded to two thiolates.<sup>15,21</sup> These theoretical interpretations, however, also need realistic molecular simulations to validate.

In the present study we perform atomistic driven dynamics simulations for a gold–benzenedithiolate (BDT)–gold molecular junction to probe the critical information on its structural evolution and breaking forces under pulling. To make the simulations more realistic to incorporate the long-range elasticity of gold electrodes, we employed a simple driven

Received: March 24, 2015

Revised: June 5, 2015

Published: June 5, 2015

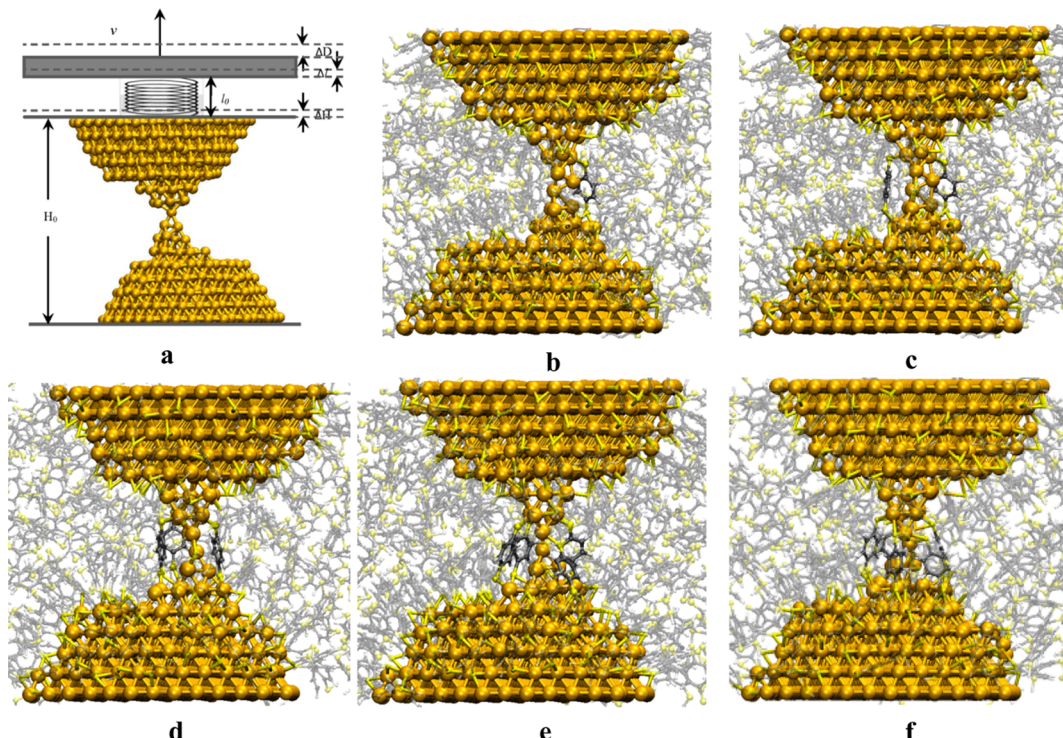


**Figure 1.** Molecular binding configurations of BDT on gold electrodes. (a) Schematic representation of a driven dynamics model applied to a gold nanojunction. (b–f) Au–BDT–Au molecular junctions containing one- to five-bridging BDT molecules. These molecular binding configurations are obtained after 1, 2, 4, 11, and 16 millions of GCMC moves.

dynamics model<sup>22</sup> in this study. The initial molecular binding structure of the Au–BDT–Au junction was obtained through the Grand-Canonical Monte Carlo (GCMC) simulation. We show that there exists an intimate correlation between the force–distance trace and the structural evolution of the Au–BDT–Au junction. The force–distance curves and the associated breaking force histograms obtained from the driven dynamics simulations reveal many remarkable features observed in the break junction experiments.<sup>3–6</sup> The intermediate break junction structures obtained from these simulations could be immediately used for subsequent molecular transport calculations that would eventually close the force–structure–conductance loop.

In the following, we briefly describe molecular models and basic simulation methods, followed by the detailed simulation results and discussion. We focus on the detailed breaking force traces and the associated structural evolutions of different Au–BDT–Au molecular junctions under pulling. Preliminary electron-transport calculations for a few intermediate break junction structures are also presented, which support the idea of conductance transition we proposed through this study.

## 2. MOLECULAR MODELS AND SIMULATION METHODS

**2.1. Grand-Canonical Monte Carlo Simulation.** The GCMC simulations are performed in a constant  $\mu$ V ensemble in which the chemical potential  $\mu$  for BDT molecules is determined to fit its bulk density at 298 K.<sup>19</sup> GCMC moves include insertion and deletion as well as translational and rotational sampling of BDT molecules, with the four types of moves attempted with equal probability of 1/4. Interatomic interactions for the gold–organic system include (1) the gold–gold interactions described by the semiempirical second-

moment approximation of the tight-binding (TB-SMA),<sup>23</sup> (2) the BDT–BDT interactions described by the universal force field (UFF),<sup>24</sup> which includes the intramolecular (such as the bond stretching, bond angle bending, dihedral angle torsion and inversion, as well as the nonbonded van der Waals, and electrostatic terms) and intermolecular interactions (the electrostatic and van der Waals interactions), and (3) the BDT–Au interactions described by the Au–S bonded chemical potentials (parametrized from the DFT calculations for metal–organic interactions<sup>25,26</sup>) and the Au–BDT nonbonded interactions described by the UFF.<sup>24</sup> During the GCMC moves, the BDT molecules are allowed to interact with gold atoms through either nonbonded or bonded potentials, depending on the S–Au distance. If the S atom is within the chemical bonding distance of an Au atom on the gold electrode, the bonded interaction potentials will be activated, while the nonbonded potentials will be turned off. At the same time, the H atom originally bonded to S atom will be removed. Here we apply a simple cutoff distance ( $r_c = 2.869 \text{ \AA}$ ) to judge whether the Au–S interaction is chemical bonding or nonbonded interaction. This is based on the equilibrium fluctuation of the Au–S bond length at room temperature, which gives a 99.73% confidence of all of the Au–S bond length fluctuating around  $r_{\text{Au–S}} = 2.4 \text{ \AA}$ .<sup>25</sup> Au–S bond breaking in GCMC simulation, namely, removing inappropriate Au–S bonding, is realized through the GCMC deletion move. Monte Carlo sampling of translational moves for gold atoms are also performed during GCMC simulation, allowing Au–S binding geometry to evolve and thiolate molecules to migrate on gold electrodes.

**2.2. Driven Dynamics Simulation of Molecular Junction under Pulling.** To explore the nature of the dynamic evolutions of molecular binding structures and breaking forces of metal–molecule–metal junction under

pulling, we begin with a stable elastic contact between two gold electrodes (composed of a total of 832 Au atoms) whose jump-to-contact and jump-out-of-contact<sup>27</sup> could be well-reproduced by repeatedly approaching and pulling the upper gold electrode through a driving-spring model.<sup>22</sup> Here the long-range elasticity of the upper gold electrode could be represented by a driving spring connected to a driving support (Figure 1a), and the pulling speed is set to  $v = 1$  m/s, which is much lower than those used in DFT-MD simulations of Au–alkanedithiolate–Au<sup>18</sup> and Au–BDT–Au junctions.<sup>15</sup> We use a double-reversible reference system propagator algorithm (double-RESPA) to propagate the metal–organic system.<sup>19</sup> The temperature is controlled at 298 K by the standard Nosé–Hoover thermostat. We use the Gear backward algorithm to integrate the dynamic equations of motion of the upper gold electrode. The bond migration of BDT on gold is realized through frequent updating of the S–Au bonding pairs by every 20 MD time steps, with the time step  $\Delta t = 2$  fs. The spring force constant  $k_z$  is set to 15.7 N/m according to the experimental fitting in MCBJ,<sup>27</sup> however, this value is also comparable to the AFM cantilever spring force constant.<sup>3,5</sup>

All of the molecular simulations are performed with our modified computational codes employed in our previous GCMC and MD studies.<sup>19,22</sup>

### 3. SIMULATION RESULTS AND DISCUSSION

**3.1. Self-Assembly of BDT Molecules on Gold.** We first investigate the self-assembly of BDT molecules on the gold single-atom contact by the GCMC simulations. After 16 million GCMC moves with intermittent MD relaxations, a saturated BDT self-assembled monolayer (SAM) on gold with five bonded BDT bridging molecules is formed in a bulk BDT liquid (Figure 1f). These five BDT bridging molecules are attached to the gold neck, along with a SAM of BDT on the two gold electrodes. Table 1 shows the detailed information on

**Table 1. Summary of the Simulation Results of the Self-Assembly of BDT on Gold**

number of GCMC moves (million)	number of bridging molecules	number of monolayer molecules	number of bulk liquid molecules
1	1	94	191
2	2	109	206
4	3	116	207
11	4	137	205
16	5	140	206

the self-assembly at different GCMC sampling stages. Other unsaturated binding structures in different stages of GCMC moves are shown in Figure 1b–e, which consist of one to four bridging BDT molecules and SAM on gold. Monte Carlo sampling of gold atoms is also allowable, resulting in the configuration changes of metal contact upon the formation of SAM on gold (Figure 1b–f).

Careful examination of the thiolate-gold binding structure shows that there are 246 surface gold atoms involved in Au–S chemical bonding, from which 65 Au atoms form the distinct RS–Au–SR structures on gold electrodes (Figure 2). This particular Au–SR<sub>2</sub> structure was observed by recent scanning tunneling microscopy (STM) for alkanethiolate SAM on the Au (111) surface.<sup>28</sup> Moreover, we find that the number of S–Au on-top binding is far less than that of on-bridge binding. As

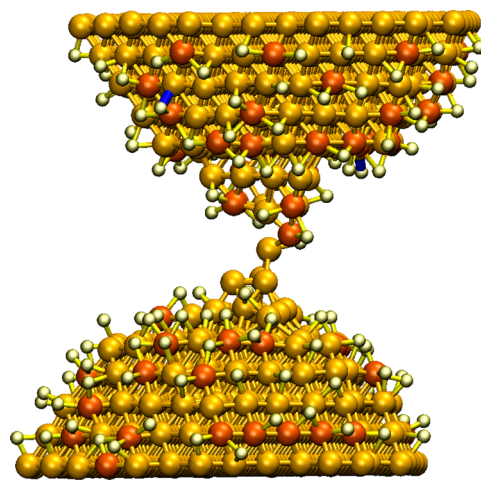


**Figure 2.** S–Au binding configuration when a BDT SAM is formed on gold electrodes. Au and S are shown in gold (or brown) and white, respectively. The surface gold atoms involved in RS–Au–SR units are shown in brown. The on-top Au–S bonds are shown in blue and on-bridge Au–S bonds are shown in yellow.

shown in Figure 2, out of ~280 S–Au bonds in BDT SAM, only two binding sites are on-top binding (the blue Au–S bond), suggesting that the on-bridge binding of BDT on the curved Au surface is more favorable.

**3.2. Breaking Force Traces and Structural Evolutions of Molecular Junctions under Pulling.** To study the breaking force variation and the associated dynamic evolution of molecular binding structures under pulling, we perform driven dynamics simulations by stretching the driving spring to mimic the force measurement in AFM.<sup>22</sup> Before pulling, all nonbonded BDT molecules in bulk liquid are removed, similar to the evaporation of sample solution before the conductance measurements are performed.<sup>7,11</sup> We assume that only the bridging BDT molecules and the SAM in the vicinity of gold electrode contact are directly involved in the dynamic evolution of molecular binding structures and breaking forces. A total of 250 independent simulation runs of pulling are performed, with 50 for each binding configuration containing one to five bridging BDT molecules. In Figure 3, we show two typical force traces for one-bridging BDT (the least saturated) and five-bridging BDT (the saturated) binding structures from driven dynamics simulations. Force traces for the two-, three-, and four-bridging BDT binding structures are provided in the Supporting Information Figure S1. These sawtooth force traces (the blue lines) exhibit a number of force jumps due to the rearrangements of gold atoms or the S–Au bond migrations near the Au–BDT–Au molecular junction. According to the procedure of building breaking-force histogram in AFM,<sup>3,5</sup> the sawtooth force traces should be converted to stepwise force curves (the red ones in Figure 3), which consist of a series of force plateaus that correspond to the original force ramps. Here the height of each force plateau is the summation of the subsequent force jumps. In this way, each force plateau represents the nominal breaking force required to induce subsequent structural rearrangements of the molecular junction prior to the final bond rupture. This “accumulation treatment” of force jumps provides a straightforward definition of breaking forces of molecular junctions at different pulling stages, yielding a different perspective of understanding the mechanical properties of metal–molecule–metal junctions under pulling.

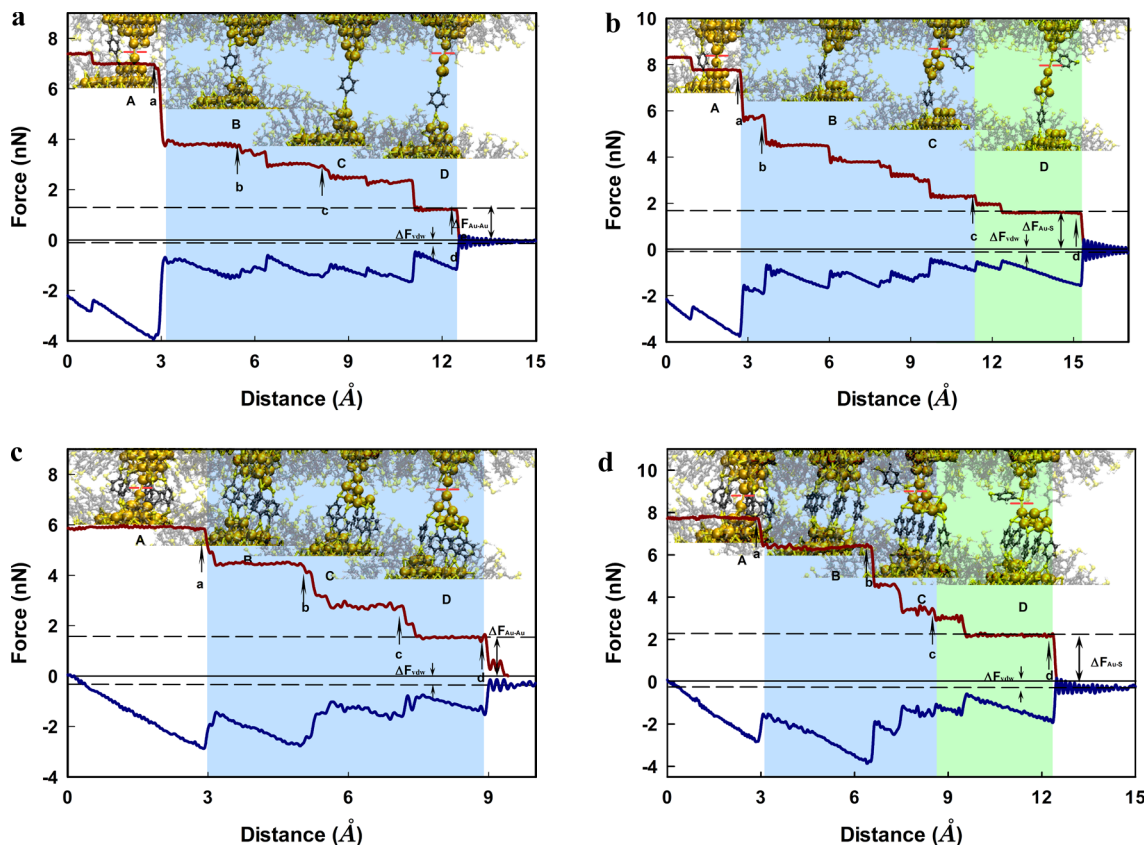


**Figure 3.** Breaking force traces of molecular junctions. (a,c) and (b,d) are for the type I Au–Au and the type II Au–S bond rupture cases, respectively, for the one- and five-bridging BDT molecular junctions. The original force traces are drawn in blue sawtooth curves, while the converted force traces are shown in red stepwise curves. Au, C, S, and H are shown in gold, gray, yellow, and white, respectively. The locations of bond rupture are represented by small red bars in the inset molecular configurations. The light-blue and light-green shaded areas represent the high-conductance and the low-conductance junctions, respectively.

**Table 2. Average Stiffness ( $k_{\text{eff}}$ ) and Pulling Distances ( $\Delta$ ) of Molecular Junctions**

bridge molecule and bond rupture	initial gold contact $k_{\text{eff}}$ (N/m)	pulling dist. $\Delta$ (Å)	final rupture $k_{\text{eff}}$ (N/m)	pulling dist. $\Delta$ (Å)
1	Au–Au	$9.32 \pm 0.18$	$2.69 \pm 0.23$	$4.92 \pm 0.82$
	Au–S	$9.39 \pm 0.19$	$2.74 \pm 0.13$	$3.68 \pm 0.26$
2	Au–Au	$6.62 \pm 0.64$	$2.39 \pm 0.22$	$3.72 \pm 0.89$
	Au–S	$6.52 \pm 0.13$	$2.42 \pm 0.17$	$2.74 \pm 0.85$
3	Au–Au	$8.15 \pm 0.40$	$2.28 \pm 0.16$	$5.33 \pm 1.14$
	Au–S	$8.41 \pm 0.47$	$2.40 \pm 0.25$	$3.11 \pm 1.03$
4	Au–Au	$7.91 \pm 0.67$	$2.56 \pm 0.28$	$5.02 \pm 0.17$
	Au–S	$8.38 \pm 0.01$	$2.67 \pm 0.10$	$3.27 \pm 0.01$
5	Au–Au	$10.04 \pm 0.39$	$2.49 \pm 0.35$	$4.68 \pm 0.33$
	Au–S	$10.44 \pm 0.14$	$2.63 \pm 0.32$	$3.27 \pm 0.47$

In Figure 3a–d, we show that the initial pulling always results in the first breakdown of the gold electrode contact (the inset configuration B), leaving a net Au–BDT–Au molecular junction. Subsequent pulling results in essentially two distinct types of force traces. Type I force traces, which come from ~80% of the total simulation runs (Figure 2a,c), correspond to the Au–Au bond rupture at final breakdown (see Supporting Information Table S1). This Au–Au bond is very close to the Au–BDT–Au junction, indicating that the Au–S bond is stronger than the Au–Au bond.<sup>4</sup> The pulling distance of the one-bridging BDT junction (~12.4 Å, Figure 2a) is much longer than that of the five-bridging BDT binding structure (~8.8 Å, Figure 2c). We attribute this to the rigidity of the multibridging BDT molecules in the molecular junction. This

trend is also seen for the two-, three-, and four-bridging BDT binding structures; however, the initial pulling distances prior to the rupture of the gold electrode contact fluctuate only slightly between 2.28 and 2.74 Å for these molecular junctions (see Table 2, Figure 2, and the Supporting Information Figure S1). The final breaking force  $\Delta F_{\text{Au–Au}}$  is ~1.5 nN, consistent with early measurements of Au–Au bond rupture.<sup>3,4,29</sup> Type II force traces, which come from the remaining 20% simulation runs (Figure 3b,d), exhibit much longer pulling distances than those of type I due to the formation of an additional alternating gold–thiolate chain<sup>15</sup> near the Au–BDT–Au junction. Carefully tracking the formation of this gold–thiolate chain, we find that it could be originated from either the S–Au on-bridge binding or the RS–Au–SR binding unit in the initial GCMC

equilibrium configuration. Initially, the side BDT molecule is bonded to two Au atoms in a small gold chain (configuration C in Figure 2b,d). As the pulling continues, the Au–Au bond in the chain breaks first, resulting in a polymeric “–Au–SR–Au–” unit (configuration D in Figure 2b,d). The final breaking force  $\Delta F_{\text{Au-S}}$  is  $\sim 2$  nN, corresponding to the rupture of one of the Au–S bonds in the “–Au–SR–Au–” unit. This breaking force is much larger than the Au–Au bond strength. Note that both  $\Delta F_{\text{Au-Au}}$  and  $\Delta F_{\text{Au-S}}$  include a small force contribution from the van der Waals attraction,  $\Delta F_{\text{vdw}}$ , which gradually decays to zero during the final rupture of molecular junctions.

Following the experimental protocol of building breaking-force histogram<sup>3–5</sup> in Figure 4, we plot the Au–Au and Au–S

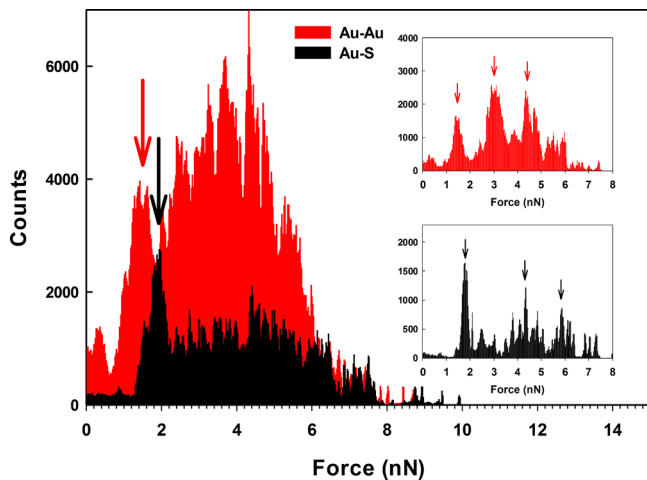


**Figure 4.** Au–Au (type I) and Au–S (type II) bond-breaking force histograms from a total of 250 simulations. Arrows in the Figure are placed as visual guides to the force peaks in approximately 1.5 and 2 nN force quanta. The two insets in the Figure show the histograms from a group of selected samples for the Au–Au and Au–S bond rupture, corresponding to remarkable force peaks at force quanta of 1.5 and 2 nN, respectively.

bond rupture force histograms from the type I and type II converted force traces. The final breaking force peaks at 1.5 and 2 nN for the Au–Au and Au–S bond rupture are clearly seen in the Figure, indicating that the Au–S bond is much stronger than the Au–Au bond; however, because of the small computational sample and randomness, the subsequent force peaks are not quite obvious. As a usual practice in experiments, we further reconstruct the histograms from a small group of force traces that represent typical force curves in simulations. As shown in the insets in Figure 4, the small sample histograms exhibit remarkable peaks at force quanta of 1.5 and 2 nN, respectively. (See the Supporting Information Table S1.) We attribute these two force quanta to the force jumps largely from the rearrangements of gold atoms for the Au–Au bond breaking and from the S–Au bond migrations for the Au–S bond breaking. (See the Supporting Information animation movies.) Because the Au–S bond formation and breaking in the “–Au–SR–Au–” unit are observed with a small fraction ( $\sim 20\%$ ) in our simulations, we anticipate that the force peak for Au–S bond breaking in AFM break junction measurements<sup>3,4</sup> could be easily masked by the total force measurements, in which the event of Au–Au bond breaking was dominant.<sup>7</sup>

### 3.3. Proposed Conductance Transition versus Structural Changes of Molecular Junctions under Pulling.

From various experimental conductance measurements<sup>7,9,11,30,31</sup> and molecular transport calculations<sup>13,15,16,20</sup> for the Au–BDT–Au molecular junctions, we propose a scenario of the conductance transition for the Au–BDT–Au molecular junctions under pulling. According to Figure 3, prior to the rupture of the gold electrode contact the conductance is around  $1G_0 = 2e^2/h \approx 77.5 \mu\text{S}$  (quantum of conductance). The contributions to the total conductance from the bridging BDT molecules, which can be considered as parallel circuits, will be small. As the gold electrode single-atom contact breaks, the net Au–BDT–Au junction emerges and the conductance transition will essentially follow the two types of force traces shown in Figure 3. Type I force traces (Figure 3a,c) correspond to a high-conductance state before breakdown, which is on the order of  $0.1G_0$  due to the direct electrode–BDT–electrode contact. This was previously measured<sup>11,30,31</sup> and verified theoretically by the DFT calculations.<sup>13,15,16,20</sup> In particular, as the molecular junctions are significantly stretched (accompanied by a few force jumps due to the rearrangement of gold electrode; see configurations B, C, and D in Figure 3a,c), the conductance could be slightly higher due to the formation of gold monatomic chains.<sup>20</sup> For the saturated BDT binding structure in which five-bridging BDT molecules exist in the Au–BDT–Au junction (Figure 3c), the conductance of molecular junction could be even higher due to the possible effect of constructive interference.<sup>32</sup> This high-conductance state directly switches to a zero-conductance state upon the rupture of the Au–Au bond.

Type II force traces (Figure 3b,d) involve the transitions from a high-conductance to a low-conductance state, during which the conductance is changed from  $\sim 0.1G_0$  to the order of  $\sim 0.01G_0$  upon the formation of the “–Au–SR–Au–” unit adjacent to the Au–BDT–Au junction. The low conductance of this specific Au–SR–Au–BDT–Au structural unit has been confirmed by recent DFT calculations when the BDT molecule is decoupled from the direct contact from the two gold electrodes.<sup>15</sup> This low conductance around  $0.01G_0$  was often observed in previous experiments.<sup>9,11</sup> Type I and II force traces indicate that out of the high-conductance states ( $\sim 0.1G_0$ ) of Au–BDT–Au molecular junctions,  $\sim 20\%$  of which can be switched to the low-conductance states ( $\sim 0.01G_0$ ) under pulling, owing to the formation of the “–Au–SR–Au–” unit. This occurrence probability seems consistent with the experimental measurements by Tsutsui et al.<sup>11</sup> for the gold–BDT–gold junction and by Aradhya et al. for the gold–bipyridine–gold junction.<sup>5</sup> The low probability of high-to-low conductance transition from our simulations also supports the experimental measurements by Li et al. for the gold–octanedithiolate–gold junction,<sup>4</sup> in which they found the high-conductance (H) to the low-conductance (L) transition has a very low probability, and when both were observed in the same curve, they showed that the L step always occurred right after the H step; however, the explanation for the high-to-low conductance transition, that is, the binding geometry changes due to the S migrations from the “on-hollow” to the “on-top” site of S–Au binding, was not supported by recent DFT calculations.<sup>13,15,20</sup> More complicated binding structures involving multiple “–Au–SR–Au–” units<sup>15</sup> were not found in our simulations, which may correspond to the even lower molecular conductance state.<sup>7</sup>

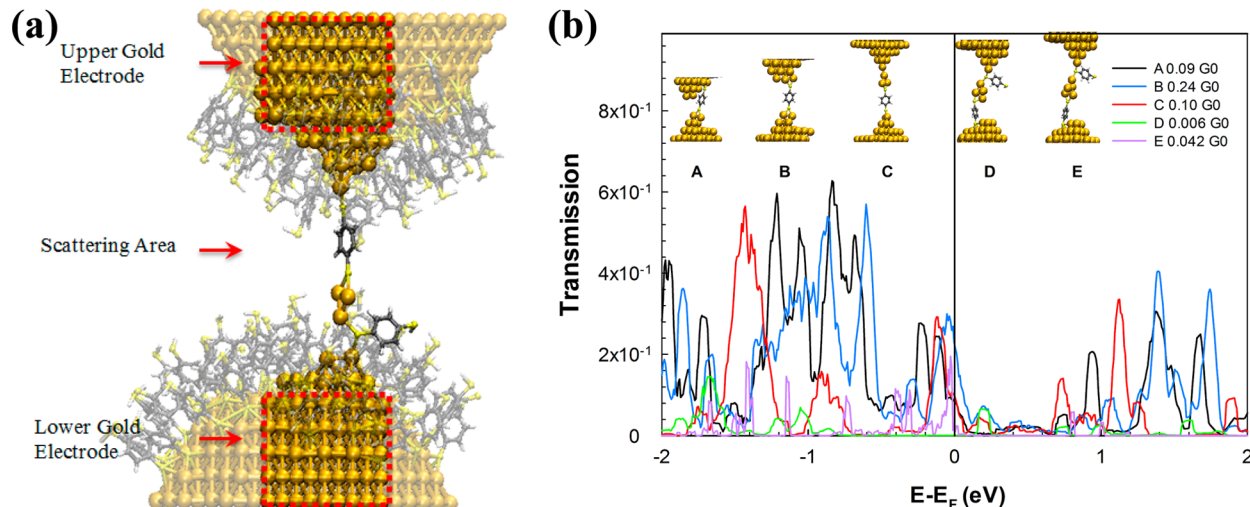


**Figure 5.** Electron-transport calculations for the Au–BDT–Au molecular junctions. (a) Extracted computational super cell including two gold electrodes (enclosed in red dotted squares) and the scattering region of local Au–BDT–Au junction. (b) Transmission functions for Au–Au (configuration A, B, and C) and Au–S (configuration D and E) bond breaking of one-bridging BDT molecular junctions.

To further test the idea of conductance transitions that correspond to the two types of force traces, we have performed preliminary electron-transport calculations for a few selected one-bridging BDT molecular junctions. The computational super cell is shown in Figure 5a, in which all of the monolayer BDT molecules and the gold atoms far away from molecular junction are removed to save computational time. The electronic structure calculations are performed using the atomic orbital DFT code SIESTA<sup>33</sup> with the Perdew–Burke–Ernzerhof (PBE) exchange-correlation functional. The mesh cutoff defining the real-space grid used is 200 Ry. We employ the single- $\zeta$  (SZ) basis, which offers quick calculations and some insight into qualitative trends in the chemical bonding. The transport properties are calculated using the non-equilibrium Green's function method as implemented in the TRANSIESTA code,<sup>34</sup> which is built on SIESTA. The transmission is done with k-point sampling of  $(3 \times 3)$  in the  $(x,y)$  plane for the whole system. The zero-bias conductance is given by  $G = T(E_F)$ , where  $T$  is the transmission probability and  $E_F$  is the electrode Fermi level. Figure 5b shows the transmission functions of type I and type II one-bridging BDT molecular junctions at different pulling stages. The Figure clearly shows that the Au–Au bond breaking configurations (A, B, and C) have a transmission function roughly 1 order of magnitude higher than those of the Au–S bond breaking configurations (D and E). Values of conductance of these junctions at zero bias are shown in the Figure, which are generally consistent with our predictions previously discussed.

**3.4. Stiffness and Pulling Distance of Molecular Junctions.** From the type I and type II force traces, we determine the effective stiffness  $k_{\text{eff}}$  and pulling distances  $\Delta$  of different molecular junctions prior to the final rupture of Au–Au or Au–S bond. Stiffness is determined by the slope of the original force curves.<sup>3,5</sup> These results are shown in Table 2, in which we also tabulate initial stiffness and pulling distance of the gold electrode contact prior to its rupture.

Table 2 shows that the values of effective stiffness ( $k_{\text{eff}}$ ) at final rupture are less than those of initial gold single-atom contact surrounded by BDT bridging molecules (Figure 2 and Figure S1 in the SI, stage A), which vary from 6.5 to 10.4 N/m. The relative low stiffness of initial gold contact in two-bridging

BDT junction is due to an additional BDT molecule directly bonded to the gold–gold contact (shown in Figure S1 in the SI). The thermal fluctuation of this molecular entity accelerates the initial Au–Au bond breaking. Consequently, this mediated structure may result in a decrease in the stiffness of initial gold–gold contact. Because  $k_{\text{eff}}$  obtained in such a way includes the contribution of the driving spring ( $k_z = 15.7$  N/m) in series, which is equivalent to the AFM cantilever spring or the elasticity of the gold electrode in MCB,<sup>27</sup> it must be corrected as  $k_{\text{eff}}k_z/(k_z - k_{\text{eff}})$ .<sup>3,5</sup> After this correction, we find that the molecular stiffness for type I and II bond rupture has been increased to 4.9–8.1 and 3.3–4.9 N/m, respectively.

A more stringent consideration for the calculation of the actual stiffness of molecular junction is to exclude the elasticity of the gold model electrodes. For the gold nanojunction shown in Figure 1a, the total elongation or the driving distance ( $\Delta D$ ) of the gold nanojunction is composed of the driving spring elongation ( $\Delta L$ ) and the elongation of the gold model electrode (including the gold single-atom contact) ( $\Delta H$ ). For the gold dimer contact,<sup>22</sup> we find that the breaking force after elastic training of the contact is  $\sim 0.87$  nN. Because  $\Delta H$  was  $\sim 0.83$  Å at rupture and the Au–Au bond length was increased from equilibrium by only  $\sim 0.2$  Å (table II and figure 6a in ref 22), we conclude that a large part of the elastic deformation of the gold nanojunction was contributed from the banks of gold electrodes. This is consistent with other experimental analyses.<sup>27,29</sup> On the basis of a simple linear spring model, we calculate the molecular stiffness of Au–Au bond as high as 43.5 N/m, while the effective stiffness of the gold model electrodes together with the gold dimer is  $\sim 10.5$  N/m. The latter is in agreement with previously published results.<sup>3,5,29</sup> After recalibration of the effective stiffness of the gold model electrodes, we finally determined that the realistic values of the stiffness of the type I and type II Au–BDT–Au molecular junctions are in the range of 7.6–19.6 and 4.3–7.6 N/m, respectively. These results suggest that the high-conductance state (type I Au–Au bond rupture) has a higher stiffness of molecular junction than that of the low-conductance state. Interestingly, this finding is similar to the experimental findings by Aradhya et al.;<sup>5</sup> however, we attribute the high-conductance state with high stiffness to the lack of additional “–Au–SR–

Au—" unit in the molecular junction rather than to the van der Waals interactions at metal–organic interfaces.<sup>5</sup> Moreover, our calculations suggest that, in general, the stiffness of Au–BDT–Au molecular junction is far less than that of the single Au–Au bond due to the complexity of metal–organic binding structures.

#### 4. CONCLUSIONS

In the present study, we have used atomistic driven dynamics simulations to probe the breaking force and structural evolution of a metal–molecule–metal junction in MCBJ/AFM conductance/force measurements. Simulation results for the Au–BDT–Au molecular junction reveal remarkable features similar to AFM experimental force measurements. The detailed molecular binding structures associated with the two types of force traces (the Au–Au and Au–S bond rupture) are crucial to molecular transport calculations. Preliminary results of electron-transport calculations for one-bridging BDT molecular junctions are consistent with our predictions. The simulation approach and main findings reported in this paper have broad impacts on the exploration and understanding of molecular junction systems and would advance studies in molecular electronics and nanoenergy systems.

#### ■ ASSOCIATED CONTENT

##### Supporting Information

Force traces derived from driven dynamics simulations for the two-, three-, and four-bridging BDT molecular junctions under pulling, partitions of the Au–Au and Au–S bond breaking from the original 250 force traces and from a small group of representative force traces, and four animation movies for the Au–Au and Au–S bond rupture. The Supporting Information is available free of charge on the ACS Publications website at DOI: 10.1021/acs.jpcc.5b02843.

#### ■ AUTHOR INFORMATION

##### Corresponding Author

\*E-mail: leng@gwu.edu. Tel: 202-994-5964.

##### Notes

The authors declare no competing financial interest.

#### ■ ACKNOWLEDGMENTS

This work was partially supported by the National Science Foundation (NSF 1149704) and the National Energy Research Scientific Computing Center (NERSC).

#### ■ REFERENCES

- (1) Aviram, A.; Ratner, M. A. Molecular Rectifiers. *Chem. Phys. Lett.* **1974**, *29*, 277–83.
- (2) Nitzan, A.; Ratner, M. A. Electron Transport in Molecular Wire Junctions. *Science* **2003**, *300*, 1384–1389.
- (3) Xu, B. Q.; Xiao, X. Y.; Tao, N. J. Measurements of Single-Molecule Electromechanical Properties. *J. Am. Chem. Soc.* **2003**, *125*, 16164–16165.
- (4) Li, X. L.; He, J.; Hihath, J.; Xu, B. Q.; Lindsay, S. M.; Tao, N. J. Conductance of Single Alkanedithiols: Conduction Mechanism and Effect of Molecule-Electrode Contacts. *J. Am. Chem. Soc.* **2006**, *128*, 2135–2141.
- (5) Aradhya, S. V.; Frei, M.; Hybertsen, M. S.; Venkataraman, L. Van Der Waals Interactions at Metal/Organic Interfaces at the Single-Molecule Level. *Nat. Mater.* **2012**, *11*, 872–876.
- (6) Frei, M.; Aradhya, S. V.; Hybertsen, M. S.; Venkataraman, L. Linker Dependent Bond Rupture Force Measurements in Single-Molecule Junctions. *J. Am. Chem. Soc.* **2012**, *134*, 4003–4006.
- (7) Reed, M. A.; Zhou, C.; Muller, C. J.; Burgin, T. P.; Tour, J. M. Conductance of a Molecular Junction. *Science* **1997**, *278*, 252–254.
- (8) Xu, B. Q.; Tao, N. J. J. Measurement of Single-Molecule Resistance by Repeated Formation of Molecular Junctions. *Science* **2003**, *301*, 1221–1223.
- (9) Xiao, X. Y.; Xu, B. Q.; Tao, N. J. Measurement of Single Molecule Conductance: Benzenedithiol and Benzenedimethanethiol. *Nano Lett.* **2004**, *4*, 267–271.
- (10) Venkataraman, L.; Klare, J. E.; Nuckolls, C.; Hybertsen, M. S.; Steigerwald, M. L. Dependence of Single-Molecule Junction Conductance on Molecular Conformation. *Nature* **2006**, *442*, 904–907.
- (11) Tsutsui, M.; Teramae, Y.; Kurokawa, S.; Sakai, A. High-Conductance States of Single Benzenedithiol Molecules. *Appl. Phys. Lett.* **2006**, *89*, 163111.
- (12) Di Ventra, M.; Pantelides, S. T.; Lang, N. D. First-Principles Calculation of Transport Properties of a Molecular Device. *Phys. Rev. Lett.* **2000**, *84*, 979–982.
- (13) Sergueev, N.; Tsetseris, L.; Varga, K.; Pantelides, S. Configuration and Conductance Evolution of Benzene-Dithiol Molecular Junctions under Elongation. *Phys. Rev. B* **2010**, *82*, 073106.
- (14) Ke, S. H.; Baranger, H. U.; Yang, W. T. Models of Electrodes and Contacts in Molecular Electronics. *J. Chem. Phys.* **2005**, *123*, 114701.
- (15) Strange, M.; Lopez-Acevedo, O.; Hakkinen, H. Oligomeric Gold-Thiolate Units Define the Properties of the Molecular Junction between Gold and Benzene Dithiols. *J. Phys. Chem. Lett.* **2010**, *1*, 1528–1532.
- (16) Pontes, R. B.; Rocha, A. R.; Sanvito, S.; Fazzio, A.; da Silva, A. J. R. Ab Initio Calculations of Structural Evolution and Conductance of Benzene-1,4-Dithiol on Gold Leads. *ACS Nano* **2011**, *5*, 795–804.
- (17) Kamenetska, M.; Koentopp, M.; Whalley, A. C.; Park, Y. S.; Steigerwald, M. L.; Nuckolls, C.; Hybertsen, M. S.; Venkataraman, L. Formation and Evolution of Single-Molecule Junctions. *Phys. Rev. Lett.* **2009**, *102*, 126803.
- (18) Paulsson, M.; Krag, C.; Frederiksen, T.; Brandbyge, M. Conductance of Alkanedithiol Single-Molecule Junctions: A Molecular Dynamics Study. *Nano Lett.* **2009**, *9*, 117–121.
- (19) Pu, Q.; Leng, Y. S.; Zhao, X. C.; Cummings, P. T. Molecular Simulation Studies on the Elongation of Gold Nanowires in Benzenedithiol. *J. Phys. Chem. C* **2010**, *114*, 10365–10372.
- (20) French, W. R.; Iacovella, C. R.; Rungger, I.; Souza, A. M.; Sanvito, S.; Cummings, P. T. Atomistic Simulations of Highly Conductive Molecular Transport Junctions under Realistic Conditions. *Nanoscale* **2013**, *5*, 3654–3659.
- (21) Hakkinen, H. The Gold-Sulfur Interface at the Nanoscale. *Nat. Chem.* **2012**, *4*, 443–455.
- (22) Wang, H. C.; Leng, Y. S. Molecular Dynamics Simulations of the Stable Structures of Single Atomic Contacts in Gold Nanojunctions. *Phys. Rev. B* **2011**, *84*, 245422.
- (23) Cleri, F.; Rosato, V. Tight-Binding Potentials for Transition-Metals and Alloys. *Phys. Rev. B* **1993**, *48*, 22–33.
- (24) Rappe, A. K.; Casewit, C. J.; Colwell, K. S.; Goddard, W. A.; Skiff, W. M. Uff, a Full Periodic-Table Force-Field for Molecular Mechanics and Molecular-Dynamics Simulations. *J. Am. Chem. Soc.* **1992**, *114*, 10024–10035.
- (25) Leng, Y. S.; Krstic, P. S.; Wells, J. C.; Cummings, P. T.; Dean, D. J. Interaction between Benzenedithiolate and Gold: Classical Force Field for Chemical Bonding. *J. Chem. Phys.* **2005**, *122*, 244721.
- (26) Leng, Y. S.; Dyer, P. J.; Krstic, P. S.; Harrison, R. J.; Cummings, P. T. Calibration of Chemical Bonding between Benzenedithiolate and Gold: The Effects of Geometry and Size of Gold Clusters. *Mol. Phys.* **2007**, *105*, 293–300.
- (27) Trouwborst, M. L.; Huisman, E. H.; Bakker, F. L.; van der Molen, S. J.; van Wees, B. J. Single Atom Adhesion in Optimized Gold Nanojunctions. *Phys. Rev. Lett.* **2008**, *100*, 175502.
- (28) Maksymovych, P.; Sorescu, D. C.; Yates, J. T. Gold-Adatom-Mediated Bonding in Self-Assembled Short-Chain Alkanethiolate Species on the Au(111) Surface. *Phys. Rev. Lett.* **2006**, *97*, 146103.

- (29) Rubio-Bollinger, G.; Bahn, S. R.; Agrait, N.; Jacobsen, K. W.; Vieira, S. Mechanical Properties and Formation Mechanisms of a Wire of Single Gold Atoms. *Phys. Rev. Lett.* **2001**, *87*, 026101.
- (30) Bruot, C.; Hihath, J.; Tao, N. J. Mechanically Controlled Molecular Orbital Alignment in Single Molecule Junctions. *Nat. Nanotechnol.* **2012**, *7*, 35–40.
- (31) Ulrich, J.; Esrail, D.; Pontius, W.; Venkataraman, L.; Millar, D.; Doerrer, L. H. Variability of Conductance in Molecular Junctions. *J. Phys. Chem. B* **2006**, *110*, 2462–2466.
- (32) Vazquez, H.; Skouta, R.; Schneebeli, S.; Kamenetska, M.; Breslow, R.; Venkataraman, L.; Hybertsen, M. S. Probing the Conductance Superposition Law in Single-Molecule Circuits with Parallel Paths. *Nat. Nanotechnol.* **2012**, *7*, 663–667.
- (33) Soler, J. M.; Artacho, E.; Gale, J. D.; Garcia, A.; Junquera, J.; Ordejon, P.; Sanchez-Portal, D. The Siesta Method for Ab Initio Order-N Materials Simulation. *J. Phys.: Condens. Matter* **2002**, *14*, 2745–2779.
- (34) Brandbyge, M.; Mozos, J. L.; Ordejon, P.; Taylor, J.; Stokbro, K. Density-Functional Method for Nonequilibrium Electron Transport. *Phys. Rev. B* **2002**, *65*, 165401.